Rare Metal Materials and Engineering
Volume 47, Issue 6, June 2018
Online English edition of the Chinese language journal

Available online at www.sciencedirect.com
ScienceDirect

Cite this article as: Rare Metal Materials and Engineering, 2018, 47(6): 1708-1715.

ARTICLE

Corrosion Performance of W-Ni-Cu and W-Ni-Fe Alloys

Li Lu, Liu Zhu, Liu Yuxiang

University of Manchester, Manchester MB 9PL, UK

Abstract: Tungsten heavy alloys (WHAs) possess a special combination of properties, such as high density, high mechanical strength and good corrosion resistance. The corrosion performance of two WHAs, 90%W-6%Ni-4%Cu and 95%W-3.5%Ni-1.5%Fe has been investigate by immersion test and electrochemical test. The AFM results indicate the attack would be on the W phase in W-Ni-Cu alloy when it generates galvanic corrosion, while W-Ni-Fe alloy reveals an opposite result. Potentiodynamic polarization measurement shows pH value is an important factor in corrosion rate. The two types of alloys show relatively lower corrosion rates in DI water, as compared to 0.6 mol/L HCl solution. The corrosion mechanism involved in the release of the metallic components and generation of corrosion products was analyzed by SEM and EDX.

Key words: tungsten heavy alloy; corrosion; surface potential measurement; potentiodynamic polarization measurement

Tungsten heavy alloys (WHAs) are the composite materials that consist of tungsten (85wt%~99wt%) with various combinations of nickel and other elements (e.g. Cu, Fe, Cr) making up the remaining parts. These alloys are divided into W-Ni-Fe, W-Ni-Cu, W-Ni-Mn among other main series according to the composition characteristics and applications[1,2]. Tungsten parts are metal matrix composites consisting of tungsten particles embedded in a lower melting point alloy. These alloys are made by a powder metallurgy technique, which involves liquid phase sintering process[3]. Tungsten heavy alloys achieve a special combination of properties, such as high density (17~18.5 g/cm^3), low thermal expansion coefficient, good corrosion resistance and oxidation resistance, good thermal conductivity, high strength, good ductility and good impact toughness. These alloy properties are very sensitive when it comes to processing, but they become degraded as a result of residual porosities and impurities, as well as segregation and embrittlement of hydrogen, and the formation of intermetallic phase[4]. Recently, a few studies have found the methods to improve the strength and toughness of WHAs by changing materials to nano-size and nanostructure[5,6]. WHAs are now widely used in industrial and military applications which range from space systems to daily necessities. The high density components can also be used in radiation shielding applications. In addition, the military have been interested in tungsten heavy alloys since it is necessary to find the replacements for the depleted uranium in kinetic energy penetrators and lead in small arms and ammunitions because of environmental effect problems[7,8].

Mclennan and Smithells developed W-Ni-Cu alloys for the first time in 1935 which were produced by powder metallurgy techniques involving liquid phase sintering[9]. These metal powders are milled in ball mills which are blended in the required ratios by weight, then compressed and sintered at approximately 1500 °C, which is an adequate temperature to melt the binder materials but not tungsten[3]. Quenching is then used to restrain the development of intermetallic compounds such as WCo_3. Tungsten particles are embedded in a lower melting point alloy and form two different phases: the tungsten phase which has body centred cubic lattice and the binder phase which has face centred cubic lattice[6]. Discontinuity between the tungsten grains is to ensure ductility of the WHAs. Equilibrium phase diagrams manifest that tungsten has certain solubility in other metals which are used for producing alloys at sintering temperature. Thus, discovering tungsten in binder phase after cooling is expected. The composition and quantity of the metals constituting the binder phase determine the amount of tungsten in binder phase. Some studies reveal that 45 wt% is tungsten solubility in cobalt and nickel at 1480 °C and 30 wt% is tungsten solubility in iron at this temperature[10].

Received date: December 22, 2017
Corresponding author: Li Lu, Master, School of Materials, University of Manchester, Manchester M13 9PL, UK, E-mail: lennonll@126.com

However, these metals are generally insoluble in tungsten phase at that temperature. In terms of copper and tungsten, both metals are basically insoluble in each other.

Corrosion is a common process where metals coming from their elemental forms or alloys are released into the environment as known. Studies that have been so far conducted with regards to the investigations of tungsten heavy alloys corrosion are very scanty, because it has not been considered an issue, and these studies made all attempts to predict WHAs structural failure when subjected under long-term storage conditions[11-13]. However, alloys made of copper were even more prone to corrosion and other alloys as this were also proved by Z. Abdel Hamid and H. B. Hassan[14].

Therefore, in this work, the corrosion performance of two tungsten heavy alloys was investigated to determine the corrosion rate and mechanism in different aqueous solutions.

1 Experiment

1.1 Material preparation

Tungsten heavy alloy powders with composition of 90%W-6%Ni-4%Cu and 95%W-3.5%Ni-1.5%Fe were prepared by a mechanical alloying method. Pure elemental powders of tungsten, nickel, copper and iron have been mechanically alloyed in a ball mill. The prepared powders were cold compacted by hydraulic press and then were sintered using a liquid phase sintering technique in vacuum atmosphere. The sintering temperature of 90%W-6%Ni-4%Cu was 1410 °C and the sintering temperature of 95%W-3.5%Ni-1.5%Fe was 1480 °C.

1.2 Surface potential measurement

In order to measure the surface potential of tungsten phase and binder phase, Kelvin Probe Force microscopy (KPFM) is a suitable technique for measurement. For this method, 15 mm×15 mm quadrate samples were used. The samples were ground using silicon carbide papers up to grade level 2400#. After that, the samples were polished, using diamond base 3 and 1 micron, making sure all scratches were removed as much as possible. Then, the samples were cleaned using ethanol and acetone and dried. The Dimension 3100 model AFM was used in this study, the scan size of the test was about 50 μm and the scan rate was 0.5 Hz.

1.3 Electrochemical test

Tungsten heavy alloy was used as the working electrode and platinum rod as the counter electrode. Before each experiment, the exposed area of the working electrode was polished using SiC papers to grade 1200#, then washed with deionized water and dried. Then, the sides of the samples were painted by lacquer, in order to avoid any reaction with these surfaces and the crevice's corrosion. A saturated calomel electrode (SCE) was used as the reference electrode. The electrolytes were DI water or 0.6 mol/L HCl solution. Then, the polarisation test was started by first finding the open circuit potential (OCP), and after that by starting the cyclic sweep to find the Tafel line.

1.4 Immersion test

For the immersion test, specimens of 7.5 mm×15 mm rectangular were fabricated. The specimen was polished using SiC papers to grade 2400# without any scratch, then washed with deionized water and dried. The sides of the samples were also painted using lacquer, to ensure that there was no contact with the solution. The two different types of WHAs specimens were placed in separate beakers containing 200 mL DI water or 0.6 mol/L HCl solution. The setup was left for 20 d under the common experiment condition. In order to prevent evaporation of solution, the beaker was covered with a plastic wrap. After 20 d of immersion test, the samples were placed in a vacuum environment and then analysed by scanning electron microscopy (SEM) and energy dispersive spectroscopy (EDS). In addition, for the SEM and EDX analysis, a ZEISS SIGMA field emission scanning electron microscope fitted with an Oxford EDS system was used, and the acceleration voltage was 15 kV in this study.

2 Results and Discussion

2.1 Microstructure characteristics

Fig.1 shows the SEM images of the microstructures on the surface of the W-Ni-Cu alloy. This typically sintered alloy is characterized by spherical tungsten particles which are embedded in Ni-Cu binder phase. The W particle size varies from 10 μm to 50 μm, with an average size of about 30 μm. The particle size of tungsten varies due to the liquid phase sintering time, according to a study done by Shen et al[15].

The high magnification of the W phase and binder phase is shown in Fig.1b. A perfectly joint interface is noticed between W phase and Ni-Cu phase, and there is no intermetallic precipitate at tungsten or binder phases; these results are similar to those by Muddle et al's study[16]. Furthermore, it is

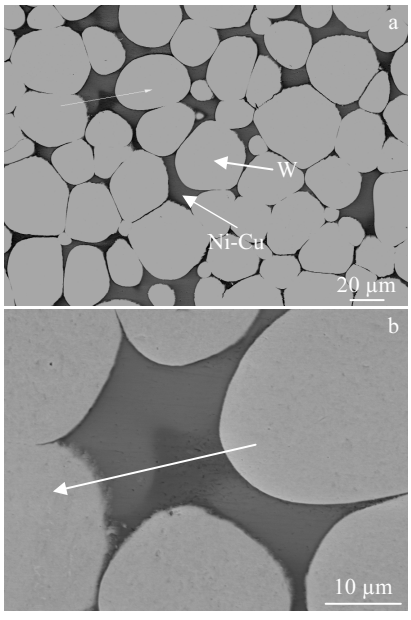

Fig.1 SEM images on the surface of the W-Ni-Cu alloy

noted that almost no small pores could be observed. At liquid-phase sintering stage, sintering temperature factor and time factor determine the number and size of pores in alloys. Shen et al. indicated that the porosity gradually decreases with an increase in sintering time[15]. Thus, the improvement of sintering temperature would reduce the porosity.

Fig.2 shows the line-scan EDS result for the selected area in Fig.1b. A certain amount of tungsten is dissolved in the binder phase. In W-rich phase, the solubility of Cu/Ni is quite low and it can be negligible. In binder phase, the solubility of W is higher, especially on the right area. The solubility of W in binder phase depends on sintering temperature, as found in the study by Mondal et al.[17] Elements Ni and Cu are not distributed evenly in binder phase, the amount of Ni is higher in bright right area and the amount of Cu is higher in dark left area with a small amount of W. This is due to low solubility of the W in Cu. According to Mondal et al's study[17], the amount of W dissolving in the Cu is about 0.04 wt%, which is quite insignificant and could be negligible, and the solubility of W in Ni is around 40 wt%. The XRD result indicates that the two phases can be identified; the bcc structured W phase and the fcc structured Ni-Cu phase, as seen in Fig.3.

Fig.4 shows the SEM images on the surface of the W-Ni-Fe alloy. The W particles are spherical in shape and different in size. Compared to W-Ni-Cu alloy, distribution of tungsten phase is more intensive in W-Ni-Fe alloy, because of the higher amount of W in alloy. From Fig.4b, it is evident that no intermediate phase could be identified between W phase and Ni-Fe phase; a similar observation was made by Zhu et al[18].

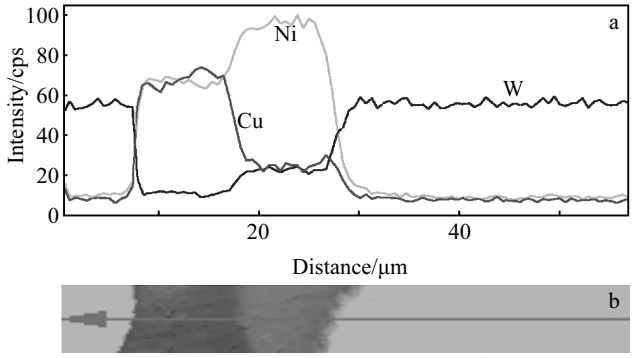

Fig.2 EDS result of the line scan (a) for selected area in Fig.1b (b)

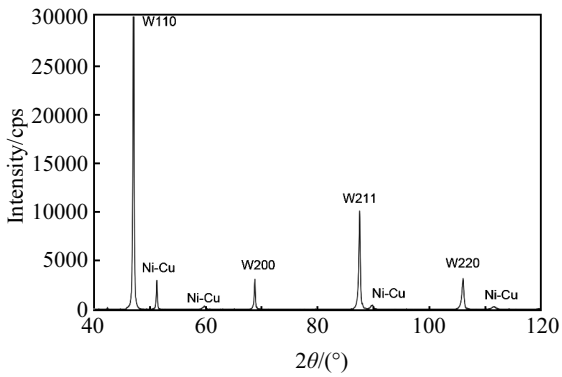

Fig.3 XRD pattern of the W-Ni-Cu alloy

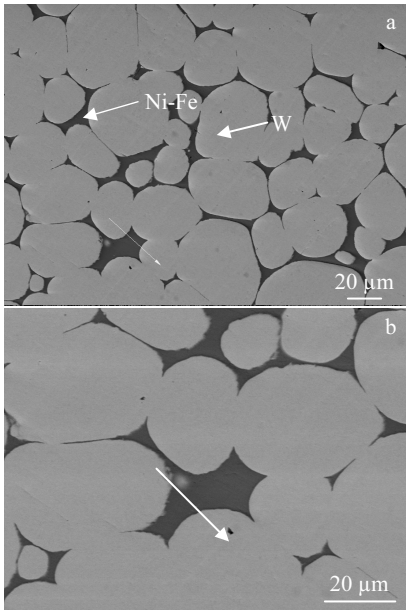

Fig.4 SEM images on the surface of the W-Ni-Fe alloy

Fig.5 shows line-scan EDS result for the selected area in Fig.4b, which indicates the amount of W and Ni-Fe dissolving in each phase. It is clear that the amount of either Ni or Fe in the W phase is quite small. On the other hand, the amount of W dissolving in binder phase is higher, as a similar result was noted by Zhu et al. where W solubility in Ni-Fe phase was around 22 wt%[18].

In Fig.5, the amount of each element between two phases has a sharp change, which indicates that interfacial phase does not exist between the W phase and Ni-Fe phase.

According to the XRD result, there are only two phases in the alloy, the bcc structured W phase and the fcc structured Ni-Fe phase, as shown in Fig.6.

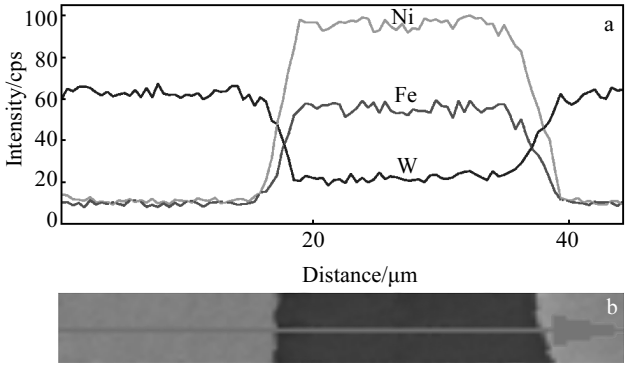

Fig.5 EDS result of the line scan (a) for selected area in Fig.4b (b)

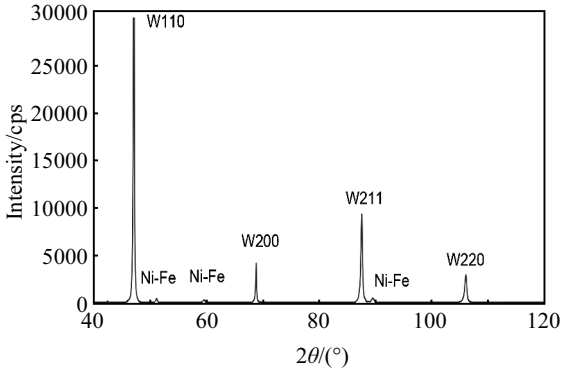

Fig.6 XRD pattern of the W-Ni-Fe alloy

2.2 Surface potential measurement

Fig.7 shows the surface potential map of W-Ni-Cu alloy. It is clear that the surface has two different regions: spherical regions are W phase area and the other region is binder phase area; the colour bar shows the difference in potential. Due to the difference in potentials of different phases, the WHAs alloys would generate galvanic corrosion in the electrolyte. According to the different values of potentials in different phases, anodic phase and cathodic phase could be identified.

Fig.8 indicates the potential line scan of W-Ni-Cu alloy for the selected line in Fig.7. It can be seen clearly that the potential of W phase is lower than binder phase, thus large area of W phase would be anode and would cathodically protect the binder phase (small area) in the alloy, and corrosion would mostly appear on the tungsten particles. Therefore, oxide of tungsten will be the major corrosion product in the DI water with a few binder elements.

The topography of W-Ni-Fe alloy is illustrated in Fig.9. As seen clearly from Fig.10 which measures the potential difference, W phase has higher potential than binder (Ni-Fe) phase. Thus, the small area of binder phase would be anode and expected to corrode first while large area of cathodic tungsten phase should be little influenced. The corrosion products mainly consist of compounds of nickel and iron because the binder phase suffers attack first.

Compared to these two WHAs alloys, the attack would be on the W particles in the W-Ni-Cu alloy. For W-Ni-Fe alloy, binder phase would be corroded first when it generated galvanic corrosion in solution.

2.3 Electrochemical test

Fig.11 is the polarization curves of the W-Ni-Cu and W-Ni-Fe sample in DI water and 0.6 mol/L HCl solutions. The results indicate that W-Ni-Cu and W-Ni-Fe alloys suffer from corrosion to a certain extent at different levels of the pH value. It is obvious that pH value plays a significant role in determi-

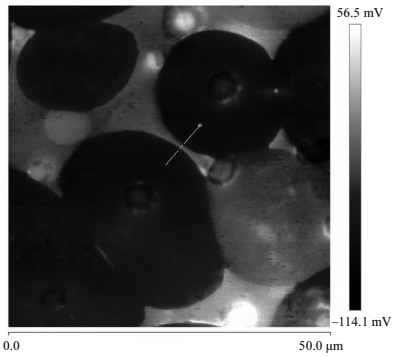

Fig.7 Surface potential map of W-Ni-Cu alloy

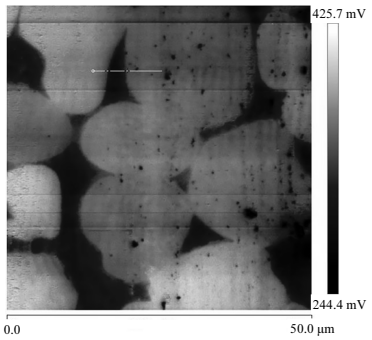

Fig.9 Surface potential map of W-Ni-Fe alloy

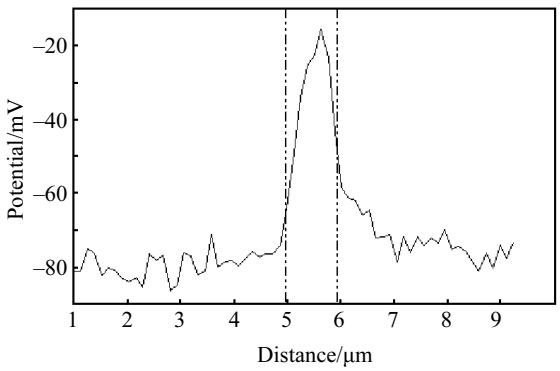

Fig.8 Potential line scan of W-Ni-Cu alloy for the selected line in Fig.7

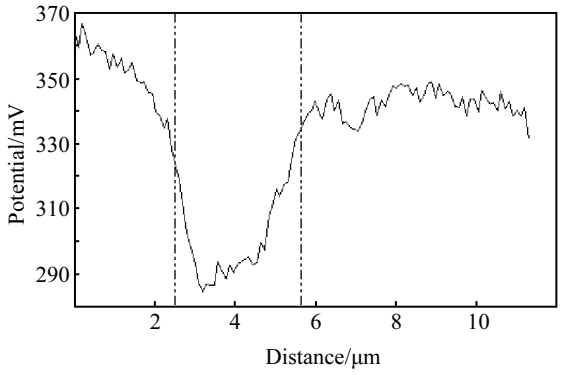

Fig.10 Potential line scan of W-Ni-Fe alloy for the selected line in Fig.9

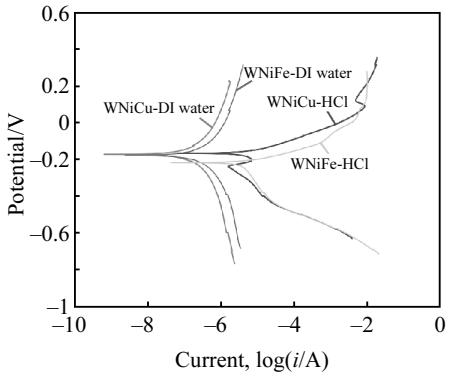

Fig.11 Polarization curves of W-Ni-Cu and W-Ni-Fe alloys in two different solutions (DI water and 0.6 mol/L HCl)

ning the corrosion rate of these alloys. Hydrogen ion could react with the surface of the alloys at the low pH value, which could change the corrosion rate to different levels. Both W-Ni-Cu and W-Ni-Fe alloys have higher corrosion rate in 0.6 mol/L HCl than in DI water, as shown in Table 1.

The following results are acquired using linear sweep voltammetry, as shown in Table 1. The two types of WHAs show the relatively lower corrosion rates in DI water. The corrosion performance of the WHAs in DI water is normally controlled by their chemical composition. It is clear that the corrosion rate of the W-Ni-Fe alloy is higher than that of W-Ni-Cu alloy, which means W-Ni-Cu alloy is less susceptible to galvanic corrosion in DI water. This may be due to the relatively high solubility of W in Ni phase as also found in the study by Ogundipe et al[19]. When the amount of dissolving W in binder phase is higher, it decreases the difference in electrode potential between the binder phase and the W phase, thus reducing corrosion rate. The amount of Ni in W-Ni-Cu alloy is higher than that in W-Ni-Fe alloy, and thus W-Ni-Cu alloy has lower corrosion rate in DI water. On the other hand, Fe could reduce the solubility of W in binder phase[20], which leads to a large difference in electrode potential between two phases; as a result, there is a higher susceptibility to galvanic corrosion.

In 0.6 mol/L HCl solution, W-Ni-Cu alloy has higher corrosion rate than W-Ni-Fe alloy, which may be due to high potential difference between the W phase and the Ni-Cu phase, and W-Ni-Cu alloy is more susceptible to galvanic corrosion. Therefore, W-Ni-Cu alloy has relatively high corrosion rate.

Table 1 Corrosion current density, Tafel slopes and corrosion rates for potentiodynamic polarization

	$\log i_{corr}$	$i_{corr}/\times10^{-7}$A·cm^{-2}	E_{corr}/V	CR/ mm·a^{-1}
WNiCu-DI water	–6.3993	3.9875	–0.1572	0.0021782
WNiFe-DI water	–6.1208	7.5718	–0.1673	0.0040450
WNiCu-0.6 mol/L HCl	–5.2954	50.652	–0.1773	0.0276700
WNiFe-0.6 mol/L HCl	–5.3725	42.413	–0.2298	0.0226576

The values of anodic and cathodic Tafel slopes were determined using Tafel extrapolation technique. Corrosion rate was also calculated using the equation below:

$$CR=Mi/nF\rho \quad (1)$$

where CR is the corrosion rate, M is the molecular mass, i is the current density, n is the number of lost electrons, F is the Farday constant, and ρ is the density of metal.

2.4 Immersion test

2.4.1 Immersion test in DI water

Fig.12 and 13 show the microstructures of W-Ni-Cu and W-Ni-Fe alloys, respectively after 20 d in DI water. It is obvious that the corrosion of W-Ni-Cu alloy begins in the W phase, and the surface of tungsten particle is very rough and binder phase is smooth, as shown in Fig.12a. This result corresponds to the AFM result, which indicates the W phase is anode and it will corrode first. Some W particles are completely dissolved in the solution, and binder phase area appears to have many small holes, where small W particles used to be. Moreover, the collapse occurs in the binder phase; this is because W particles which under the binder phase are dissolved in the solution, binder phase loses the hol der and collapses.

For W-Ni-Fe alloy, it is found that the binder phase gets most attack and the W phase has less effects, as seen in Fig.13. One interesting finding in these results is that a very thin layer has been observed between the W phase and the binder. Moreover, AFM result proves this appearance, binder phase is anode and tungsten phase is cathode, which indicates that

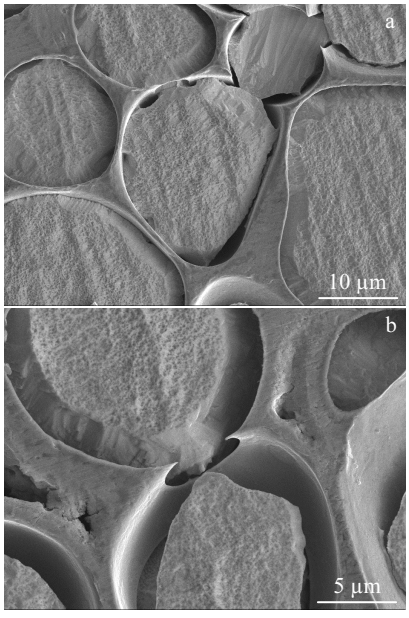

Fig.12 Microstructures of W-Ni-Cu alloy after 20 d in DI water

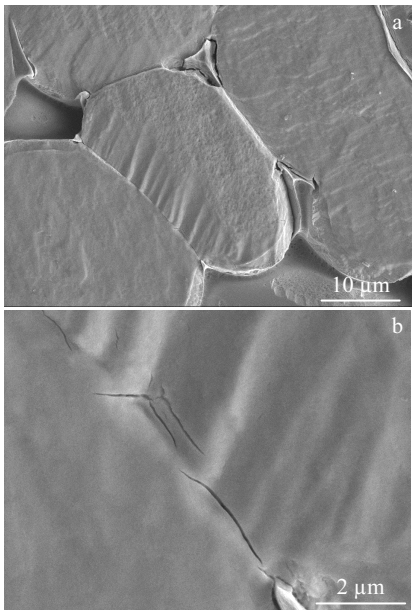

Fig.13 Microstructures of W-Ni-Fe alloy after 20 d in DI water

binder would corrode first. Due to anodic reaction of the binder phase, the possible chemical reaction would be:

$$Fe \rightarrow Fe^{2+}+2e \quad (2)$$

$$Ni \rightarrow Ni^{2+}+2e \quad (3)$$

Fig.13b shows the high magnification of tungsten phase in DI water after 20 d. It is noted that some small cracks appear on tungsten phase, which would decrease mechanical properties of the material.

2.4.2 Immersion test in 0.6 mol/L HCl solution

Fig.14 illustrates the microstructure of the W-Ni-Cu alloy, after being immersed for 20 d in 0.6 mol/L HCl solution. It can be seen that the binder phase is degraded and W phase is not affected. This result is the opposite of the immersion test in DI water and is also inconsistent with AFM result.

It is clear to note that binder phase has many small particles, which are the products of corrosion reaction between binder phase and HCl solution. In order to know the component of the particles, elemental mapping was made, as shown in Fig.15. It can be noticed that most oxygen is concentrated in

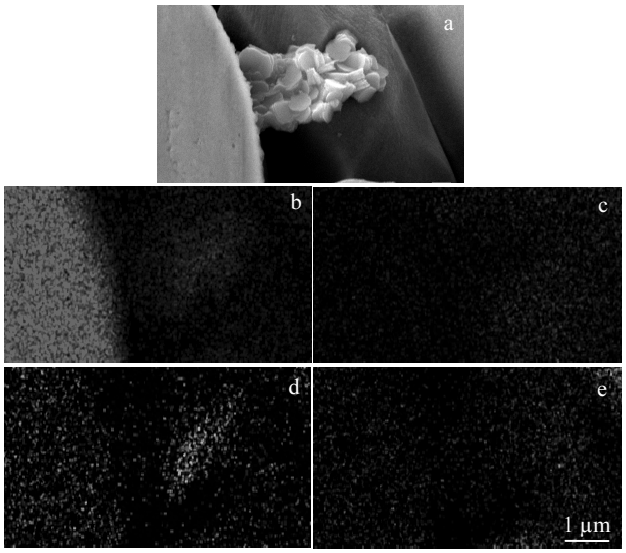

Fig.15 SEM image (a) and element mapping of W-Ni-Cu after 20 d in 0.6 mol/L HCl: (b) W, (c) Ni, (d) O and (e) Cu

the particle pile area and W is concentrated in this area and W-rich phase; meanwhile, the Ni and Cu hardly appear on the particle pile area. Therefore, these particles are tungsten oxide.

A previous study by Ogundipe et al. found that tungsten phase is dissolved and formed spherical crystal products which are converse results from this experiment when W-Cu alloy is attacked by HCl solution[19]. This may be due to df ferent immersion test methods and different binder phases in alloy.

For W-Ni-Fe alloy, Fig.16 indicates all the binder phases are gone and the positions are occupied by some corrosion products where the binder phase used to be. Almost all the empty places in binder phase area are replaced by products. It is also found that corrosion products grow on tungsten phase.

The elemental mapping of the W-Ni-Fe alloys, after 20 d from immersion test in 0.6 mol/L HCl solution, is shown in Fig.17. It is apparent to note that binder phase is attacked and replaced by products. It is found that the elements Ni and Fe are almost gone from the binder phase. In addition, most

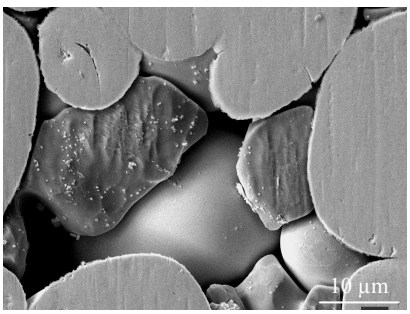

Fig.14 Microstructure of W-Ni-Cu alloy after 20 d in 0.6 mol/L HCl

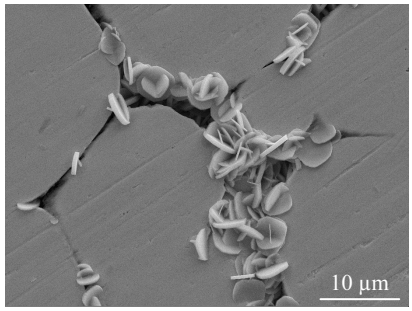

Fig.16 Microstructure of W-Ni-Fe alloy after 20 d in 0.6 mol/L HCl

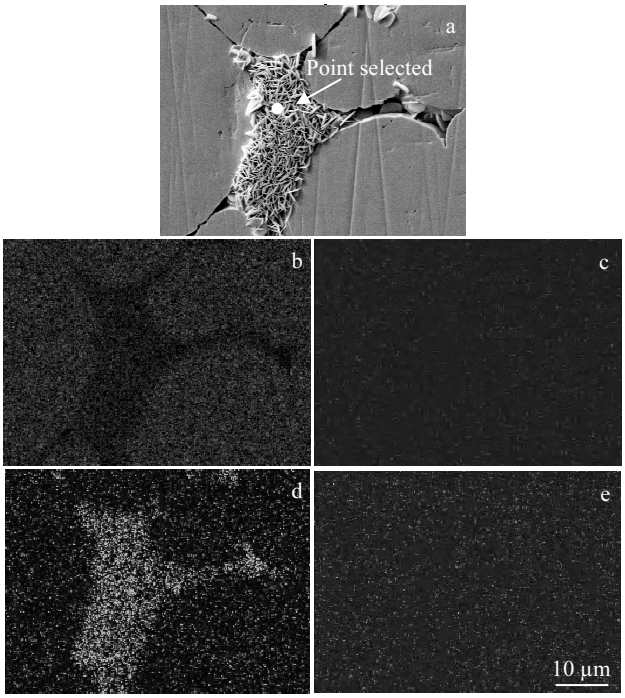

Fig.17 SEM image (a) and element mapping of W-Ni-Fe after 20 d in 0.6 mol/L HCl: (b) W, (c) Ni, (d) O and (e) Fe

Table 2 EDS result for the point scan selected in Fig.17a (wt%)

O	Fe	Ni	W	Total
28.42	0.13	0.00	71.46	100.00

oxygen is concentrated in the corrosion products area and the element W also appears in this area. From Table 2, it can be seen that corrosion products consist of W and O, with little Fe. Meanwhile, the corrosion product has a similar morphology to WO_3, as found in the study by Aslam et al[21]. Thus, the corrosion product may be WO_3.

Furthermore, it indicates that binder phase is all dissolved in the solution. This may be due to iron reacting easily with hydrogen ions, as shown in the reaction equation below:

$$Fe + 2H^+ \rightarrow Fe^{2+} + H_2 \quad (4)$$

Comparing the corrosion performance between two samples in 0.6 mol/L HCl solution, binder phase of both samples is corroded first. Additionally, they both have the corrosion products (tungsten oxide) in the binder phase area. However, for W-Ni-Fe alloy, binder phase is all dissolved and empty areas are almost fully replaced by tungsten oxide after 20 days immersion test. For W-Ni-Cu alloy, binder phase still exists after 20 d immersion test, and piles of corrosion products only appear in a few binder phase areas.

3 Conclusions

1) There is no intermediate phase identified between W phase and binder phase. The solubility of tungsten in binder phase is up to around 20wt%, but the solubility of Ni/Cu or Ni/Fe in tungsten phase is very low. The phase composition consists of two phases, bcc W phase and fcc binder phase.

2) The tungsten phase has a lower potential value than binder phase in W-Ni-Cu alloy, which means tungsten phase would behave as an anode and binder phase as a cathode. However, W-Ni-Fe alloy reveals the opposite results.

3) The corrosion rate is affected by pH value. The two types of alloys have shown a relatively lower corrosion rate in DI water, as compared to 0.6 mol/L HCl solution.

4) There is an effective degradation of tungsten phase in W-Ni-Cu alloy when it is immersed in DI water; this is due to presence of Cu, which has a relatively high potential value, causing galvanic corrosion. For W-Ni-Fe alloy, binder phase suffers attack. On the other hand, binder phases of both samples are attacked in 0.6 mol/L HCl and they both have the corrosion products (tungsten oxide) in the binder phase area.

References

1 Gero R, Borukhin L, Pikus I. *Materials Science and Engineering A*[J], 2001, 302(1): 162

2 Lee W S, Xiea G L, Lin C F. *Materials Science and Engineering A*[J], 1998, 257(2): 256

3 Khalid F A, Bhatti M R. *Journal of Materials Engineering and Performance*[J], 1999, 8(1): 46

4 Fortuna E, Sikorski K, Kurzydlowski K J. *Materials Characterization*[J], 2004, 52(4): 323

5 O'donnell R G, Woodward R L. *Metallurgical Transactions A*[J], 1990, 21(2): 744

6 Kim D K, Lee S, Baek W H. *Materials Science and Engineering A*[J], 1998, 249(1): 197

7 Pappu S, Kennedy C, Murr L E *et al*. *Materials Science and Engineering A*[J], 1999, 262(1): 115

8 Park S, Kim D K, Lee S *et al*. *Metallurgical and Materials Transactions A*[J], 2001, 32(8): 2011

9 McLennan J C, Smithells C J. *Journal of Scientific Instruments*[J], 1935, 12(5): 159

10 Chausse C, Nardou F. *Materials at High Temperatures*[J], 1999, 16(1): 37

11 Batten J J, Moore B T. *Corrosion of High-Density Sintered Tungsten Alloys. Part 2. Accelerated Corrosion Testing*, MRL-R-1145[R]. Ascot Vale: Materials Research Laboratory, 1988

12 Chang F C, Levy M, Lin S S. *The Effect of Ion Implantation on the Corrosion Behavior of a High-Density Sintered Tungsten Alloy*, MTL TR87-38[R]. Watertown: US Army Materials Technology Laboratory, 1987

13 Chang F C, Beatty J H, Kane M J *et al*. *Galvanic Corrosion of Tungsten Coupled with Several Metals/Alloys*, ARL-TR-1845[R]. Aberdeen Proving Ground: U. S. Army Research Laboratory, 1998

14 Abdel Hamid Z, Hassan H B. *Surface and Interface Analysis*[J], 2013, 45(13): 1830

15 Shen J, Campbell L, Suri P *et al*. *International Journal of Refractory Metals and Hard Materials*[J], 2005, 23(2): 99
16 Muddle B C, Edmonds D V. *Metal Science*[J], 1983, 17(5): 209
17 Mondal A, Upadhyaya A, Agrawal D. *Materials Science and Engineering A*[J], 2010, 527(26): 6870
18 Zhu Y B, Wang Y, Zhang X Y *et al*. *International Journal of Refractory Metals and Hard Materials*[J], 2007, 25(4): 275
19 Ogundipe A, Greenberg B, Braida W *et al*. *Corrosion Science*[J], 2006, 48(10): 3281
20 Lassner E, Schubert W D. *Tungsten: Properties, Chemistry, Technology of the Element, Alloys, and Chemical Compounds*[M]. New York: Kluwer Academic/Plenum Publishers, 1999
21 Aslam M, Ismail I M I, Chandrasekaran S *et al*. *Journal of Hazardous Materials*[J], 2014, 276: 120

W-Ni-Cu 和 W-Ni-Fe 合金的腐蚀性能

李　鹭，Liu Zhu，刘玉项
(曼彻斯特大学，英国 曼彻斯特 M13 9PL)

摘　要：高比重钨合金是一种具有高密度，高强度和良好的耐腐蚀性等特性的复合材料。采用沉浸试验和电化学试验对 2 种钨合金（90%W-6%Ni-4%Cu 和 95%W-3.5%Ni-1.5%Fe）的腐蚀性能进行了研究。结果表明，当 W-Ni-Cu 合金发生电偶腐蚀时，W 相首先遭到腐蚀；而在 W-Ni-Fe 合金中，粘结相会先发生腐蚀。动电位极化测量结果表明，pH 值对高比重钨合金腐蚀速率有显著影响，与酸性环境相比较，合金在中性溶液中腐蚀速率较低。根据 SEM 和 EDX 的结果分析了合金成分的溶解以及腐蚀产物的生成等腐蚀机理。

关键词：高比重钨合金；腐蚀；表面电势测量；电动位极化测量法

作者简介：李　鹭，男，1993 年生，硕士，曼彻斯特大学材料学院，曼彻斯特 M13 9PL 英国，E-mail: lennonll@126.com